Acta Materialia 181 (2019) 501–509

Contents lists available at ScienceDirect

Acta Materialia

journal homepage: www.elsevier.com/locate/actamat

Full length article

Hierarchically-structured large superelastic deformation in ferroelastic-ferroelectrics

Yu Deng[a,*], Christoph Gammer[b,*], Jim Ciston[c], Peter Ercius[c], Colin Ophus[c], Karen Bustillo[c], Chengyu Song[c], Ruopeng Zhang[c,d], Di Wu[a,e], Youwei Du[a,f], Zhiqiang Chen[g], Hongliang Dong[g], Armen G. Khachaturyan[h], Andrew M. Minor[c,d,*]

[a] Solid State Microstructure National Key Lab and Collaborative Innovation Center of Advanced Microstructures, Nanjing University, Nanjing 210093, China
[b] Erich Schmid Institute of Materials Science, Austrian Academy of Sciences, 8700 Leoben, Austria
[c] National Center of Electron Microscopy, Molecular Foundry, Lawrence Berkeley National Laboratory, Berkeley, CA 94720, United States
[d] Department of Materials Science & Engineering, University of California, Berkeley, California 94720, United States
[e] College of Engineering and Applied Sciences, Nanjing University, Nanjing 210093, China
[f] School of Physics, Nanjing University, Nanjing 210093, China
[g] Center for High Pressure Science and Technology Advanced Research, Shanghai 201203, China
[h] Department of Ceramic and Materials Engineering, Rutgers University, New Jersey 08854, United States

ARTICLE INFO

Article history:
Received 10 May 2019
Revised 24 September 2019
Accepted 4 October 2019
Available online 14 October 2019

Keywords:
Superelastic deformation
Ferroelastic-ferroelectrics
Hierarchical structure
In situ transmission electron microscope
4D-STEM

ABSTRACT

Large superelastic deformation in ferroelastic-ferroelectrics (FMs) is a complex phenomenon involving multiple mechanisms operating simultaneously. Understanding how these mechanisms contribute corporately is critical to apply this useful property to the intrinsically brittle FMs, which can therefore display both excellent functional and mechanical performance. Here, we have directly observed and quantitatively analyzed *in situ* in a transmission electron microscope the three main mechanisms of twinning domain, phase transformation and mobile point defect contributing to extremely large superelastic deformation in single-crystal $BaTiO_3$ (5.0% strain) and $Pb(Mg_{1/3}Nb_{2/3})O_3$-$PbTiO_3$ (10.1% strain). Our results reveal the hierarchical origin of large recoverable strain in "brittle" FMs.

1. Introduction

Ferroelastic-ferroelectrics have attractive next-generation applications such as flexible/wearable electronic devices, piezoelectric generators and mechanically-written high-density memory [1–4] which requires both functional and mechanical performance. While FMs are intrinsically brittle, there exist promising mechanisms that can achieve large recoverable strains through domain evolution and phase transformations [1,5,6]. For example, the ferroelastic twinning domain in $BaTiO_3$ contributes a strain (also called rubber-like strain) up to 1% (i.e. c/a-1, c and a are lattice parameters) [7]. Phase transformations can introduce even higher strain, e.g. 5% for $BiFeO_3$ through the morphotropic phase boundary transformation [8]. The superelastic deformations with simultaneously twinning domain and phase transformation enable huge recoverable strains, e.g. the 13% one in shape memory alloy Fe-Ni-Co-Al-Ta-B [9]. More, there are also reports on the surprisingly flexible nanometer FMs, in which twinning domain and phase transformation contribute accompanying with size effect [2,8,10]. Notably, in FMs the stress-induced domain evolutions and phase transformations are closely correlated, often resulting in complex hierarchical structures. As known, the multiple-phase-coexisting structures through morphotropic/thermotropic phase boundary transformation display mixed types of domain arrangements (corresponding to the different phases) [8,11,12]. And the very small bundle domains (high hierarchy twinning domains) grow inside a simple twinning domain as the multiple-axial stress loading dramatically increased [13–15]. Owing to the complex hierarchical microstructures, it is still challenging to understand the large superslastic deformation mechanisms in FMs. The domain mobility, the distributions of local strains and mobile point defects, and the growth of the bundle domain and multiple-phase-coexisting structures are all in long-time controversial [7,11–13,16–21]. Without direct *in situ* observations of the full superelastic deformation process with multiple-scale measurements, most previous researches only showed average characteristics, with many critical local features completely obscured in observations of ensembles.

* Corresponding authors.
E-mail addresses: dengyu@nju.edu.cn, aminor@berkeley.edu (Y. Deng), christoph.gammer@oeaw.ac.at (C. Gammer), aminor@lbl.gov (A.M. Minor).

https://doi.org/10.1016/j.actamat.2019.10.018
1359-6454/

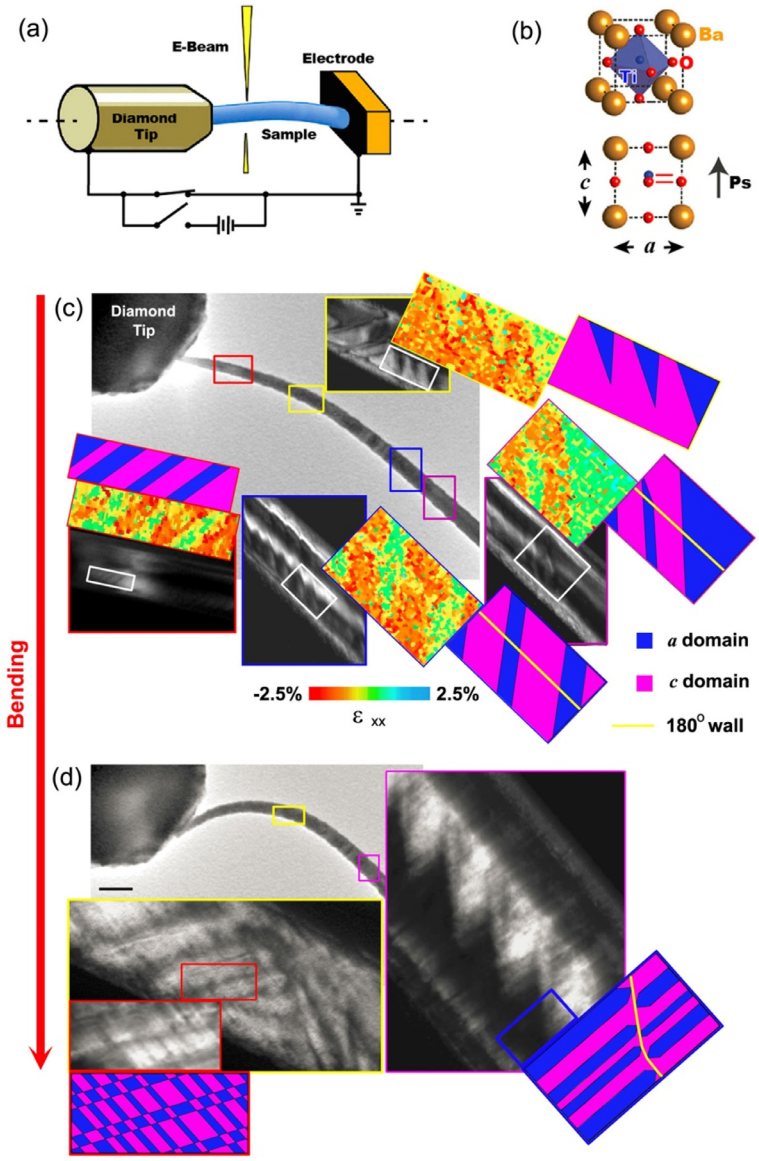

Fig. 1. (a) Schematic of the *in situ* TEM setup. It allows sample rotation for observation along different directions. The pillar's top and bottom electrodes are electrically shorted during mechanical loading, to avoid strong depolarization and charging influences. (b) Lattice models for tetragonal phase $BaTiO_3$: three-dimensional view (upper) and side-view (lower). P_S denotes spontaneous polarization. (c) The local domain and strain distributions in the $BaTiO_3$ pillar under slight bending. Each zoomed-in dark-field observation is for the region framed by the same color. Each 4D-STEM strain mapping (axial strain ε_{xx} mapping, with the corresponding domain patterns besides) is for its nearby white-framed region. To ensure a uniform orientation for dark-field TEM and 4D-STEM, we investigated the bending pillar section by section (nearly straight for each section). The 4D-STEM mapping step is 2 nm. The 180° domain walls are those between *a* and *–a*, or *c* and *–c* domains. (d) The local domain and strain distributions in the $BaTiO_3$ pillar under further heavy bending. The scale bar in (d) is 500 nm. (For interpretation of the references to colour in this figure legend, the reader is referred to the web version of this article.)

In this study, we chose free-standing single-crystal $BaTiO_3$ sub-micrometer pillar as a model system to investigate the large superelastic deformations in FMs. Single-crystal $Pb(Mg_{1/3}Nb_{2/3})O_3$-$PbTiO_3$ (PMN-PT) was chosen for further verification. The *in situ* transmission electron microscope (TEM) setup (see Fig. 1(a)) and sample preparation avoid any clamping effects and leave the sample essentially defect free except for the intrinsic mobile point defects. We focus on the stress-induced domain evolutions and phase transformations, instead of those triggered by radiation, thermal or charging effects [22]. Here the sample size (sub-micrometer) is far above the threshold (~10 nm level for $BaTiO_3$ [23]) of a size-driven structural phase transformation, which can cause significant changes in mechanical properties [24]. To directly study the deformation mechanisms *in situ*, we took advantage of high precision nanomechanical loading devices and recent advances in electron optics and direct-electron-detectors to perform four dimensional scanning transmission electron microscope (4D-STEM, with 0.1% precision, applicable from unit-cell to micrometer scale) study [25] and rapid atomic imaging [26] while the samples were under load.

2. Experimental

2.1. Sample preparation

The bulk $BaTiO_3$ and PMN-PT single crystals were purchased from Daheng Company and Siccas Companies at Shanghai, China, respectively. We fabricated the free-standing single-crystal sub-micrometer pillars by Focused Ion Beam (FIB), with the pillar axis along the main bulk crystal orientation [001] (see Fig. 1(a),(b). In

fact, there are always multiple-domain structures in bulk single crystals). To avoid strong ion-beam damage during the early FIB preparation period with strong beam currents, the samples were coated with protective Pt layers first. After FIB preparation with Ga ion beam, we further cleaned the samples' surfaces by using a Nanomill with Ar ion beam.

2.2. Characterization methods

TEM investigations were carried out by using a probe and imaging Cs-corrected (S)TEM from FEI providing sub-atomic resolution (TEAM I at NCEM) equipped with a direct-electron-detector (K2-IS, Gatan) with a size of 1920×1792 pixels and a high speed of up to 1600 frames/second. *In situ* mechanical testing was carried out using a picoindenter holder (PI-95, Hysitron). In addition, two more TEM (a Titan, FEI and a JEM-3010, JEOL) were used. All TEM observations were carried out at 300 kV. The dark-field TEM observations were performed with the diffraction $g = 404$. To limit the influence of the electron beam, we performed TEM observations using a low current density ($\leq$10–2A/cm^2), and STEM including 4D-STEM measurements were performed within a few seconds under a beam current $\leq$35pA. High-pressure Raman scattering measurements on single crystals were performed on a Renishaw inVia Raman Spectrometer system with a diamond anvil cell [27].

2.3. Simulations

Phase-field simulations and HRSTEM image simulations see supplementary materials.

3. Results and discussion

3.1. Domain evolution and mobile point defect pinning

Fig. 1(c),(d) and Movie S1 (in supplementary materials) show highly mobile domains in an as-prepared single-crystal $BaTiO_3$ pillar under bending. By dark-field TEM observations and 4D-STEM strain mapping, we found that for the slight bending case (Fig. 1(c)) there were mostly simple twinning domain patterns (composed of 90° domains and 180° domains), indicating that the pillar endures mainly uniaxial stress [28,29]. Here the simple twinning domain size is 30–100 nm. For the heavy bending case (Fig. 1(d)), there were much smaller bundle domains (hierarchical domains [13] with domain size down to a few nanometers) growing inside the simple twinning domains, to release the dramatically increased multiple-axial (i.e. axial and radial) stresses [15]. Notably, the inhomogeneous local domains in hierarchical structures are actually well integrated, adapting to the gradually changing local strains from the pillar's more compressive side (with higher c domain fraction and smaller domain size) to the other less compressive or tensile side. And owing to these local microstructures, the local strain distributions in the single-crystal pillar are inhomogeneous. It in turn promotes the inhomogeneous local domain growth and phase transformation.

Interestingly, by very slow bending (strain rate $\sim 10^{-4}$ s^{-1}, i.e. reaching a 1% strain within 100 s. see the left inset in Movie S2) we have achieved extremely large superelastic deformation (strain 5.0%, which is close to the theoretically predicted maximum recoverable strain, i.e. the maximum strain without triggering catastrophic dislocation nucleation and cracking which can cause material failure in $BaTiO_3$ [5,30]) in the as-prepared single-crystal $BaTiO_3$ pillars (with thicknesses from 100 nm to 400 nm), without introducing any dislocation/cracking. Here, the local strain ε for the bending pillar is calculated through the equation [31]

$$\varepsilon = R/\rho \quad (1)$$

where R is pillar radius and ρ is local bending curvature radius. However, if the loading strain rate is increased to $\sim 10^{-2}$s^{-1} (i.e. reaching a 1% strain within 10 s, which is far from the threshold causing any high-strain-rate effect), the large strain (~5.0%) cannot be achieved "safely" anymore (i.e. without triggering any dislocation/cracking, see Movie S2). It implies that there is a time-dependent mechanism (it works at the time scale of 100 s), which plays a critical role in the large superelastic deformation. As shown in Fig. 2(a) and Movie S3, by *in situ* TEM investigations on the full deformation processes we have discovered an time-dependent mobile-point-defect-pinning effect (it works for 100 s or longer) in the single-crystal $BaTiO_3$ pillar: For the case with strain rate $\sim 10^{-2}$ s^{-1} (with ignorable pinning effect, see the first cycle in Movie S3), the stress-induced domains in the pillar fully retract upon unloading; However for the case with strain rate $\sim 10^{-4}$ s^{-1} (with obvious pinning effect, see the second cycle in Movie S3), the stress-induced domains have been well maintained after unloading. For the later loading cycle, there is enough time for mobile point defects (mainly $V_{\ddot{O}}$ for $BaTiO_3$ [7,32]) to redistribute at the "new" domain walls, acting as pinning centers (see Fig. 2(b)) [7]. Low-angle-annular-dark-field (LAADF) and high-angle-annular-dark-field (HAADF) HRSTEM observations [33] on the pinned domain walls (see Fig. 2(c), Figure S1 and Figure S2) further show that besides the accumulated mobile point defects there are no other pinning centers such as dislocations or planar defects, which actually cannot be induced by the low stress (75 MPa). Here, the bent/strained ferroelastic domain walls (i.e. the "highways" for $V_{\ddot{O}}$ redistribution [34]) greatly enhance the pinning effect (see Fig. 2(b)). They have overcome the slow $V_{\ddot{O}}$ diffusion ($\boldsymbol{\tau}_D = 1.14 \times 10^9$s) and drifting ($\boldsymbol{\tau}_\mu = 1.61 \times 10^5$s) in $BaTiO_3$ [32], which are responsible for the slow traditional aging processes by thermal or electrical loading (hours or even days are needed) [1,7]. Of course, size effect also contributes to an easier domain pinning, owing to the much lower domain wall energy for the smaller domain size ($\gamma \propto \lambda^2$,γ is domain wall energy and λ is domain size [18]). In addition, the electron beam radiation effect here (with a low beam current density $\leq 10^{-2}$A/cm^2, and a short observation/probing time of a few seconds) causes only weak influences [22]. In fact, under such low beam current the local oxygen vacancy distribution in the insensitive FMs like $BaTiO_3$ and $SrTiO_3$ can be quantitatively studied by using high resolution TEM/STEM [33,35]. They indicate that the migration of oxygen vacancies by electron beam should be very weak in this work.

Importantly, the enhanced mobile-point-defect-pinning effect changes both domain structuring and phase transformation (it will be discussed next) [11,12]. It strongly limits the domain side growth and merging, changing the typical domain growth way of nucleation, forward growth, side growth and merging step by step [36] into another way mainly through domain nucleation and forward growth (see Figure S3). As a result, it maintains the high-density domain walls and phase boundaries, in fact enabling the hierarchically structuring in FMs. The motion and inhomogeneous distribution of point defects greatly contributes to the large superelastic deformation, which is intimately-coupled with the domain evolution and phase tranformations. Balke and Halinin et al. have reported large reversible local strains (i.e. changes in local volume) in $LiCoO_2$ that is caused by point defect drifting during the electrical cycling [37]. Similarly, during the stress-induced hierarchical domain evolution and phase transformation in $BaTiO_3$, the formation of new domain walls (see Fig. 1) and the phase boundaries (see Fig. 3) triggers $V_{\ddot{O}}$ redistribution and accumulating at the domain wall/phase boundary. The point defect itself can cause a large recoverable strain (1% level) [38]: a $V_{\ddot{O}}$ in $BaTiO_3$ lattice ($a = b = 3.996$ Å, $c = 4.036$ Å) generates O inward atomic motion of 0.04 Å for the Ba-O and 0.15 Å for the Ti-O_2 layers, as well as cationic outward motion of 0.11 and 0.06 Å for Ba and Ti

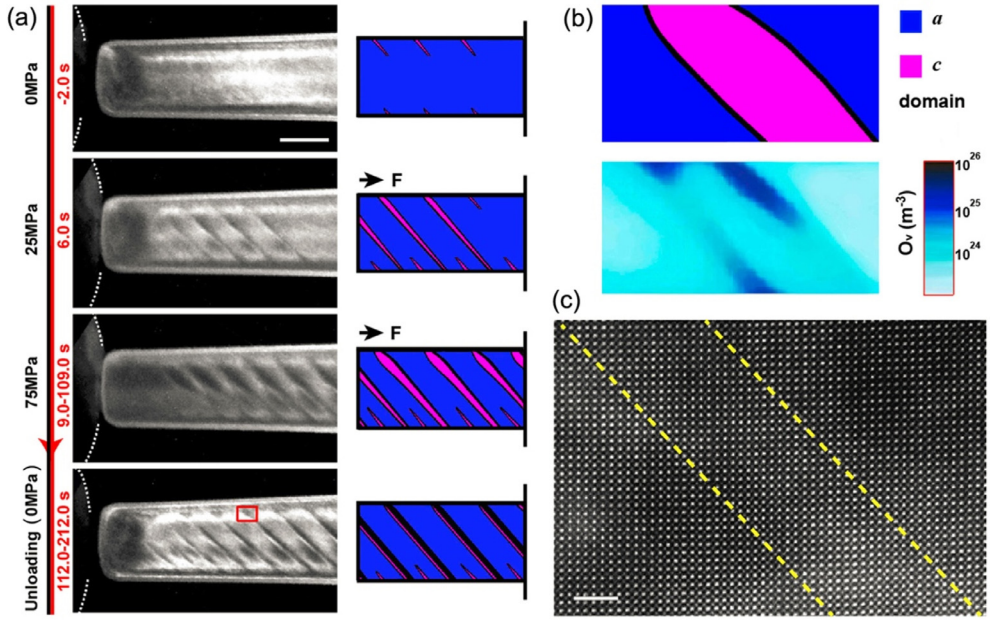

Fig. 2. A time-dependent mobile-point-defect-pinning effect. (a) Dark-field TEM observations of the domain pinning process under a slow compression loading (corresponding to the second cycle in Movie S3). The diamond tip is highlighted by white dotted lines. The right simplified models illustrate the corresponding domain structures in the pillar. (b) The phase-field simulation of the accumulated V_O at the strained (bent) 90° domain walls. (c) The LAADF HRSTEM observation on the pinned domain walls (the red-framed one in (a)). The scale bar in (a) is 100 nm and in (c) is 2 nm, respectively. (For interpretation of the references to colour in this figure legend, the reader is referred to the web version of this article.)

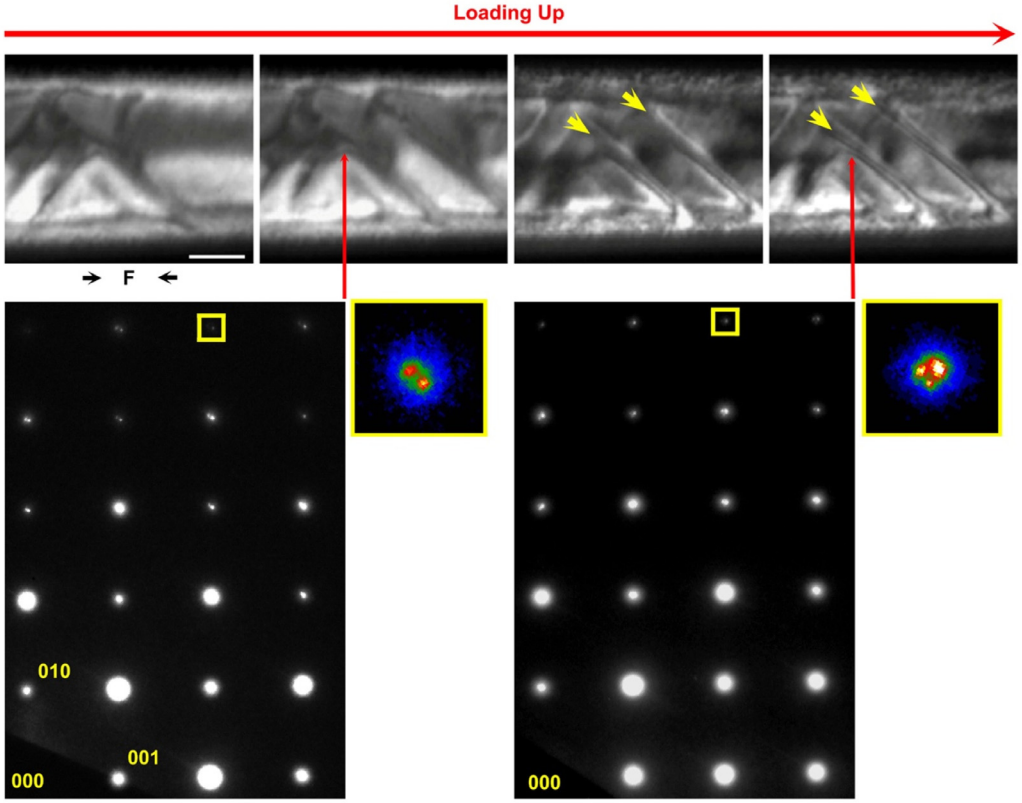

Fig. 3. The stress-induced ultrathin multi-layered structures (highlighted by yellow arrows) which nucleate at pinned 90° domain walls as compression loading up (pillar shearing is induced). And there are also 90° and 180° domain evolutions, leading to corresponding dark-field TEM contrast changing. The two lower insets show the SAED patterns at a domain wall before and after the multi-layered structures' emerging (the yellow-framed zoom-in views show the splitting diffraction spots), respectively. To clearly show the diffraction spots, we show only 1/4 of the full diffraction patterns. The scale bar is 50 nm. (For interpretation of the references to colour in this figure legend, the reader is referred to the web version of this article.)

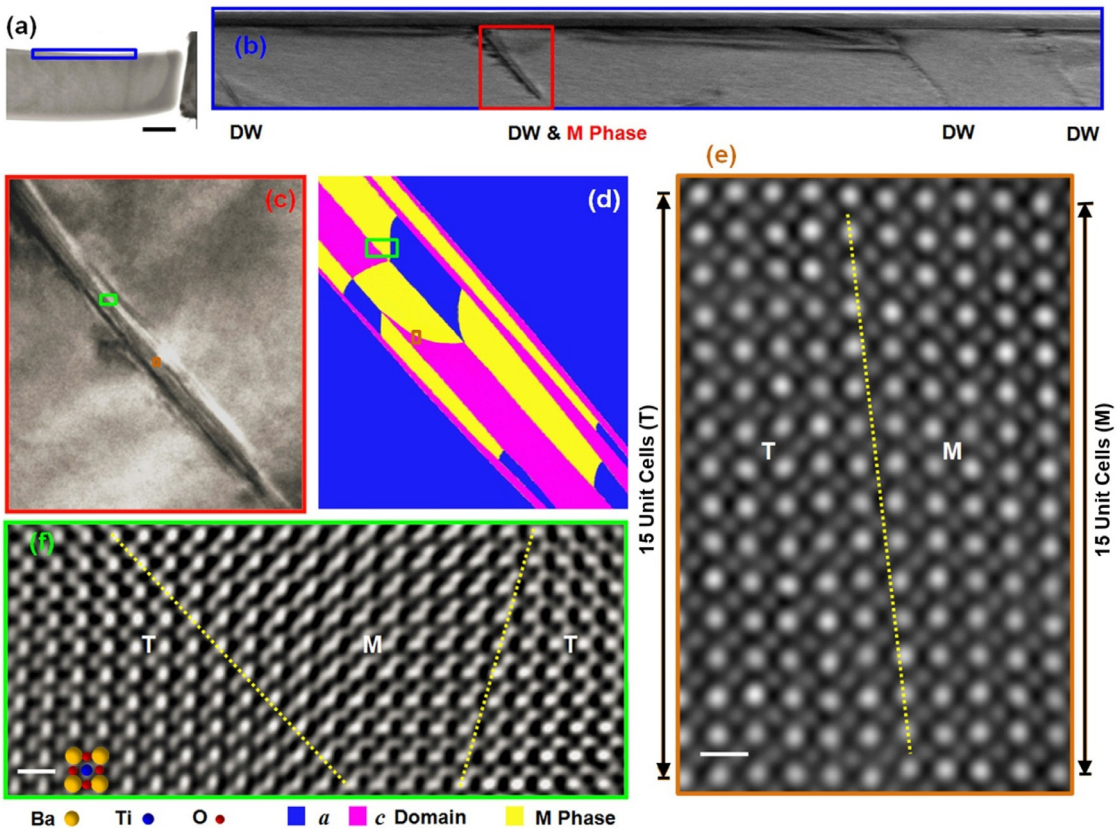

Fig. 4. Atomic resolution observation of the multiple-phase-coexisting structures nucleated at 90° domain walls. (a) A thin $BaTiO_3$ platelet under compression (shearing is induced). (b) The zoom-in observation on the platelet edge (corresponding to the same-shape blue frame in (a)), showing the pure domain walls (DW) and the ultrathin multi-layered multiple-phase-coexisting structures. (c) A further zoom-in on the multiple-phase-coexisting structures (corresponding to the same-shape red frame in (b)). (d) The phase-field simulation of the multiple-phase-coexisting structures (with Tetragonal (T) and Monoclinic (M) phases). (e) and (f) are the negative Cs (−15 μm) HRTEM observations on the multiple-phase-coexisting structures, corresponding to the same-shape green and brown frames in (c) and (d), respectively. The phase boundaries between M and T phases are highlighted by dotted yellow lines in (f) and (e). For (3), the left and right black solid lines show lattice difference of the two phase: a 1.3% difference, i.e. a 0.2 unit cell's difference for 15 unit cell. The scale bar is 500 nm for (a) and 5 Å for (e) and (f), respectively. (For interpretation of the references to colour in this figure legend, the reader is referred to the web version of this article.)

atoms, respectively [39]; and the clustered oxygen vacancies prefer to introduce local composition and phase structural transformation [33,35], also leading to large strain.

3.2. Phase transformation and multiple-phase coexistence

As expected, we found that stress-induced phase transformation was triggered in the single-crystal $BaTiO_3$ pillar as the load was further increased. Fig. 3 shows that some ultrathin multiple-layered structures (highlighted by yellow arrows) nucleate and then grow at some 90° domain walls, as the local compression stress reaching 520 MPa (the local stress is measured by 4D-STEM, see Figure S4. Here the $BaTiO_3$ pillar here is unavoidably sheared under the large compression). Notably, the 90° domain walls hardly display any side growth or merge since they are pinned by mobile point defects [13,32]. Considering the morphology of the ultrathin multiple-layered structures which is obviously not belong to any type of the nine bundle domain arrangements (for tetragonal phase $BaTiO_3$) [13], as well as the unique growth way (without growing into twinning domains [14,36]), we suggest that the ultrathin multiple-layered structures are neither simple domain nor bundle domain structures. In good agreement, the selected area electron diffractions (SAED, in two lower insets of Fig. 3) show that a monoclinic phase has been induced [12], displaying the splitting diffraction spots besides the 90° domains' (for tetragonal phase $BaTiO_3$).

To confirm the phase transformation at atomic scale, we ion-polished a $BaTiO_3$ pillar into a thin platelet (~18 nm thick at its edges, suitable for high-resolution observations) and compressed it (pillar shearing was induced) until the ultrathin multiple-layered structures emerged (Fig. 4(a),(d)). Sub-atomic resolution HRTEM observation (Fig. 4(e)) shows the lattices difference of the two phases (tetragonal (T) and monoclinic (M) ones), which agrees well with the SAED (Fig. 3) and phase field simulation (Fig. 4(d)) results. Here the M phase should be a bridging phase at the tetragonal-orthorhombic thermaltropic phase boundary [12]. And thanking to the negative Cs HRTEM observations which can distinguish 0.1° level local crystal orientation tilting in $BaTiO_3$ owing to the sensitive relative image shifting between the oxygen and Ba/Ti [40], Fig. 4(f) reveals the high-density domain walls and phase boundaries in multiple-phase-coexisting structures (averagely a few unit cells width). It contributes to large deformation through the three-dimensional local shearing [41].

According to Samara, for the $BaTiO_3$ bulk crystal the tetragonal-orthorhombic phase boundary at 520 MPa should be −5 °C [42], which is a lower temperature than relevant for this work (15 °C). Here, owing to the multiple-nanodomain and multiple-phase structures, the phase boundary can be extended to ~100 K, instead of a very sharp onset [12,43]. Moreover, it has been recently confirmed that there is a monoclinic bridging phase (Mc) at the tetragonal-orthorhombic phase boundary: The multiple-phase coexistence at this phase boundary actually displays

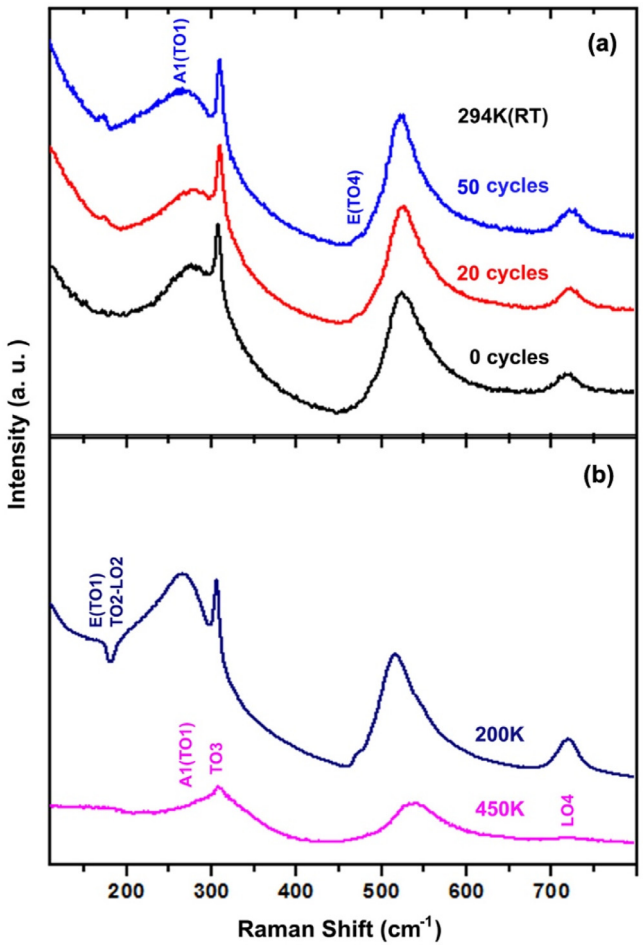

Fig. 5. (a) Raman spectra of a $BaTiO_3$ single crystal in a diamond anvil cell before and after slow cyclic compressions at 520 MPa. (b) The comparison Raman spectra of a $BaTiO_3$ single crystal measured at 200 K (rhombohedral-phase-dominated) and 450 K (cubic-phase-dominated), respectively.

three possible cases: orthorhombic-monoclinic, orthorhombic-monoclinic-tetragonal, and monoclinic-tetragonal [12]. Therefore, the monoclinic-tetragonal phase coexistence at 520 MPa and 15 °C is relevant for this work.

To further verify this 'unusual' stress-induced phase transformation (compared to the 'usual' tetragonal-to-cubic one [44]), which has been reported to be related to the multiple-pathway phase transformation or called phase re-entrance [21,45,46], we performed high-pressure Raman scattering study (by using diamond anvil cell [27]) on a $BaTiO_3$ single crystal at room temperature. As shown in Fig. 5(a), under cyclic compressions at 520 MPa with strain rate $\sim 10^{-4} s^{-1}$ (to introduce the enhanced mobile-point-defect-pinning effect and local shearing deformation), the Raman peaks' variations of $A_1(TO_1)$ (~240–270 cm^{-1}, its intensity increases and width is broadened) and $E(TO_4)$ (~485 cm^{-1}, it emerges then gradually increases) indicate that a tetragonal-orthorhombic thermaltropic phase boundary transformation has been triggered [45–47]. Notably, here the Raman spectra show neither typical rhombohedral phase Raman peaks such as the $E(TO_1)$ or TO_2-LO_2 one (see the rhombohedral-phase-dominated Raman spectrum measured at 200 K, in Fig. 5(b)) [45–49], nor the typical cubic phase Raman peaks which show obvious weakening at $A_1(TO_1)$, TO_3 and LO_4 (see the cubic-phase-dominated Raman spectrum measured at 450 K, in Fig. 5(b)) [45,47–49]. Therefore we conclude that there is little rhombohedral or cubic phase being introduced after the cyclic compressions, in good agreement with the above TEM studies.

Importantly, the hierarchically-structured multiple-phase-coexisting structures, i.e. the ultrathin multiple-layered structures, are actually also hetero-structures by the alterative different phases (see Fig. 4(d)). The pinned domain walls at where the stress-induced new phase nucleates subsequently become phase boundaries, which are well stabilized by both the mobile-point-defect-pinning effect and the multiple domain structures [12]. The intrinsically metastable multiple-phase-coexisting structures are thus stable. More, the concentration of the accumulated $V_{Ö}$ at the domain walls or phase boundaries are only of ~0.1%, even after the redistribution reaching the balance (see Fig. 2(b). It is far from the threshold (~7%) to cause any dislocation or planar defect nucleation (leading to cracking/failure) [50]. Therefore, the ultrathin multiple-phase-coexisting structures in fact greatly promote the ferroelastic strengthening effect [5,6], effectively prohibiting dislocation/cracking nucleation and growth.

3.3. A hierarchically-structured model for the large superelastic deformation

Based on above results, the extremely large superelastic deformation in single-crystal FMs (e.g. 5.0% strain for $BaTiO_3$) under the slow mechanical loading can be explained as follows: Firstly, nonlinear strains are directly provided by the domain evolution (1% strain for $BaTiO_3$ [7]) and phase transformation (1.3% strain for $BaTiO_3$ [12,43]), respectively. Secondly, under the slow loading (e.g. strain rate $\sim 10^{-4}$ s^{-1}), the mobile-point-defect-pinning effect is greatly enhanced since $V_{Ö}$ can be sufficiently redistributed to the stress-induced domain walls and act as pinning centers. As a result, the enhanced pinning effect strongly limits domains' side growth and merging, leading to the hierarchically-structured domain (with much smaller bundle domains growing inside simple twinning domains, instead of the large-size single domain through merging [36]) and multiple-phase-coexisting structures (nucleate at the pinned domain walls). Of course, the mobile point defect motion itself can introduce large local recoverable strains (1% level). Thirdly, the ultrathin domain and multiple-phase-coexisting hetero-structures dramatically promote the ferroelastic strengthening effect [5,6] in the single-crystal $BaTiO_3$. On one hand, dislocation nucleation inside an individual ultrathin domain or multiple-phase-coexisting hetero-structure is strongly depressed. For example, Matthews-Blakeslee formula predicts that a 5.2% large elastic strain is still 'safe' (i.e. without dislocation nucleation for both the main dislocation directions of <100> and <110>) [30] for a 2.4nm-

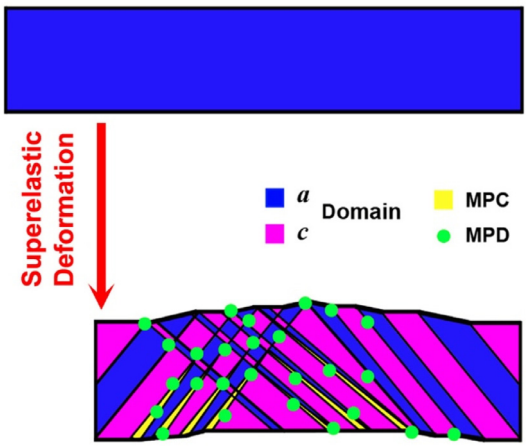

Fig. 6. A hierarchically-structured model for the large superelastic deformation in FMs. Here 'MPC' represents multiple-phase-coexisting structure and 'MPD' represents mobile point defect.

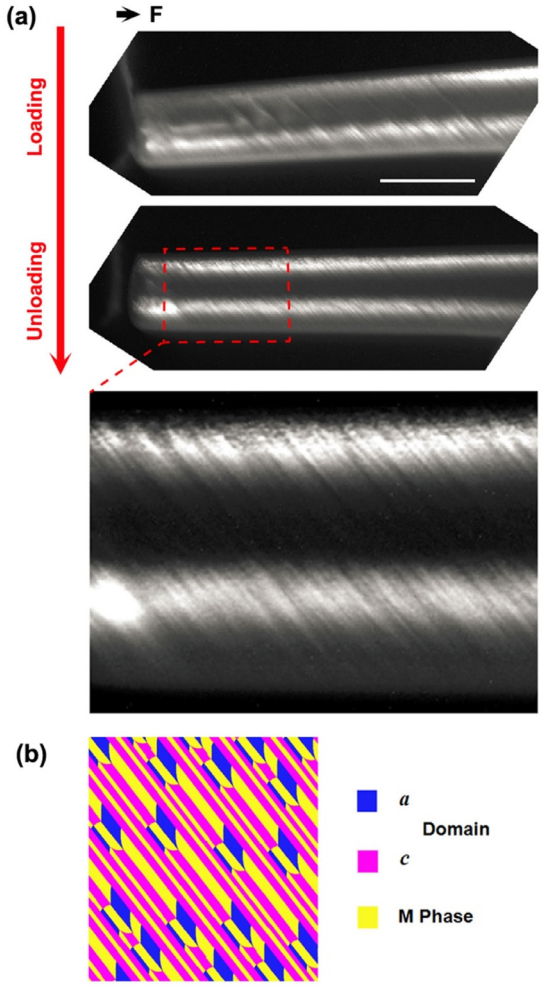

Fig. 7. (a) A 0.6 μm-thick single-crystal $BaTiO_3$ pillar with ultrathin domain and multiple-phase-coexisting structures through "mechanically engineering", i.e. 50 cycles' slow compressions (strain rate $\sim 10^{-4}s^{-1}$, at 520 MPa). (b) The phase field simulation for the ultrathin domain and multiple-phase-coexisting structures. The scale bar in (a) is 1 μm.

thin layer (we chose the value since it is the thinnest one we have observed in this study) in the single-crystal $BaTiO_3$ domain or multiple-phase-coexisting hetero-structures. On the other hand, although the domain walls or phase boundaries with high-concentration $V_{Ö}$ also cause cracking, for well crystallized single-crystal $BaTiO_3$ it can be ignored since the accumulated $V_{Ö}$ are only of ~0.1% concentration (see Fig. 2(b)) which is far from the threshold (~7%) to trigger any defect structure for failure [50]. We suggest that it is a fatigue problem only after long-time using. In sum, the extremely large superelastic deformation (i.e. the extremely large recoverable strain) of the hierarchically-structured single-crystal $BaTiO_3$ is provided by both the nonlinear part (through domain evolution and phase transformation) and the greatly enhanced elastic part (through ferroelastic strengthening effect). Additionally, the size effect should contribute to the large superelastic deformation if the FMs' size is below ~10 nm level [1,23].

As shown in Fig. 6, we present a hierarchically-structured model composing of simple twinning domains, much smaller bundle domains, and ultrathin multiple-phase-coexisting structures, to illustrate the large superelastic deformation in 'brittle' FMs. Conceptually, no matter what size the single-crystal FMs are, the large superelastic deformation is achievable as long as the ultrathin domain and multiple-phase-coexisting structures have been formed. Encouragingly, the ultrathin domain and multiple-phase-coexisting structures are always available through the "proper" high stress loading, since stress field is unscreenable in FMs [1]. As a verification, a 0.6 μm-thick single-crystal $BaTiO_3$ pillar (see Fig. 7, the center part of the pillar is too thick for electron beam transparent) has been "mechanically engineered" (i.e. introducing the ultrathin domain and multiple-phase-coexisting structures via slow cyclic compressions).

Extremely large superelastic deformation is possible via bending. The relaxor PMN-PT has an ultra-small domain structure (owing to its ultralow domain wall energy) and morphotropic phase boundary structure at room temperature, which can therefore support large hierarchically-structured superelastic deformation [1,18,27]. It has previously been shown that even for bulk single crystal PMN-PT, a large recoverable strain of 1.7% can be measured [51]). Here, we achieved a huge superelastic deformation (10.1% strain) in a 0.5μm-thick single-crystal PMN-PT pillar (Fig. 8), under a slow bending (strain rate $\sim 10^{-4}s^{-1}$). The magnified images inset in Fig. 8 show the sub-micrometer domain structures and the ultrathin multiple-phase-coexisting structures (~nm wide) [12,52,53]) inside the PMN-PT pillar, indicating that hierarchical domain and phase transformation structures have been formed.

4. Conclusions

In this paper, we studied the extremely large superelastic deformation in single-crystal FMs, by using sub-atomic resolution *in situ* TEM, Raman scattering equipped with a diamond anvil cell, and phase field simulation. The main conclusions are as follows:

(i) The extremely large superelastic deformations (with 5.0% strain for $BaTiO_3$ and 10.1% for PMN-PT, respectively) can

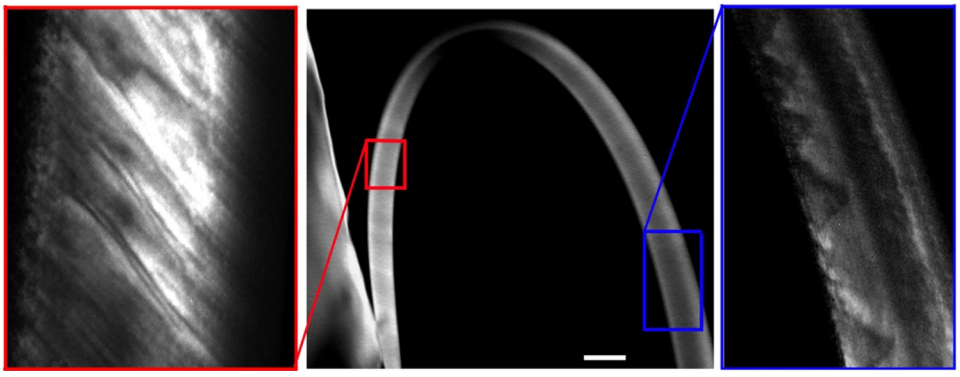

Fig. 8. Large superelastic deformation of a 0.5 μm-thick single-crystal PMN-PT pillar under a slow bending (strain rate $\sim 10^{-4}s^{-1}$). The two insets are the magnified observations, showing the sub-micrometer domain structures (right) and the ultrathin multiple-phase coexisting structures (left), respectively. The scale bar is 500 nm.

be achieved in "brittle" single-crystal FMs through slow mechanical loading (strain rate $\sim 10^{-4}$ s^{-1}).

(ii) During the large superelastic deformations, hierarchically-structured simple twinning domains, much smaller bundle domains and ultrathin multiple-phase-coexisting structures have been introduced into single-crystal FMs. The ultrathin hierarchical structures dramatically enhance the ferroelastic strengthening effect. Here, the domain evolution, phase transformation, mobile point defect, and the large elastic deformation (without dislocation and cracking) corporately contribute to the extremely large recoverable strain.

(iii) An enhanced mobile-point-defect-pinning effect under the slow loading is critical for the large hierarchically-structured superelastic formation. The pinning effect strongly limits domain side growth and merging, subsequently drives the domain miniature and the ultrathin multiple-phase-coexisting structures. Importantly, the point defect motion itself also provides a 1% level large strain.

(iv) Although size effect can contribute to superelastic deformation in FMs, here the large hierarchically-structured superelastic deformation is independent on sample size. It's valid as long as the ultrathin domain and multiple-phase-coexisting structures have been introduced in FMs.

Declaration of Competing Interest

None.

Acknowledgments

The authors acknowledge support by the National Natural Science Foundation of China (Grants Nos. 50802039) and Natural Science Foundation of Jiangsu Province, China (Grant Nos. BK20151382), and the National Science Foundation through the STROBE Science and Technology Center. RZ acknowledges funding from the US Office of Naval Research under Grant No. N00014-12-1-0413 and N00014-17-1-2283. The electron microscopy work was performed at the Molecular Foundry, Lawrence Berkeley National Laboratory, which is supported by the U.S. Department of Energy under Contract # DE-AC02-05CH11231. J.C. Acknowledges additional support from the Department of Energy Early Career Research Program.

Supplementary materials

Supplementary material associated with this article can be found, in the online version, at doi:10.1016/j.actamat.2019.10.018.

References

[1] G. Catalan, J. Seidel, R. Ramesh, J.F. Scott, Domain wall nanoelectronics, Rev. Modern Phys. 84 (2012) 119–156, doi:10.1103/RevModPhys.84.119.
[2] J.X. Zhang, B. Xiang, Q. He, J. Seidel, R.J. Zeches, P. Yu, S.Y. Yang, C.H. Wang, Y.H. Chu, L.W. Martin, A.M. Minor, R. Ramesh, Large field-induced strains in a lead-free piezoelectric material, Nat. Nanothechnol. 6 (2011) 97–101, doi:10.1038/nnano.2010.265.
[3] Y. Yang, J.H. Jung, B.K. Yun, F. Zhang, K.C. Pradel, W. Guo, Z.L. Wang, Flexible pyroelectric nanogenerators using a composite structure of lead-free $KNbO_3$ nanowires, Adv. Mater. 24 (2012) 5357–5362, doi:10.1002/adma.201201414.
[4] H. Lu, C.W. Bark, D. Esque de los Ojos, J. Alcala, C.B. Eom, G. Catalan, A. Gruverman, Mechanical writing of ferroelectric polarization, Science 336 (2012) 59–61, doi:10.1126/science.1218693.
[5] Y. Gaillard, A. Hurtado Macías, J. Muñoz-Saldaña, M. Anglada, G. Trápaga, Nanoindentation of $BaTiO_3$: dislocation nucleation and mechanical twinning, J. Phys. D. 42 (2009) 085502, doi:10.1088/0022-3727/42/8/085502.
[6] A. Kelly, N.H. Macmillan, Strong Solids, Oxford University Press, New York, 1986.
[7] X. Ren, Large electric-field-induced strain in ferroelectric crystals by point-defect-mediated reversible domain switching, Nat. Mater. 3 (2004) 91–94, doi:10.1038/nmat1051.
[8] R. Zeches, M. Rossell, J. Zhang, A. Hatt, Q. He, C. Yang, A. Kumar, C. Wang, A. Melville, C. Adamo, G. Sheng, Y. Chu, J. Ihlefeld, R. Erni, C. Ederer, V. Gopalan, L. Chen, D. Schlom, N. Spaldin, L. Martin, R. Ramesh, A strain-driven morphotropic phase boundary in $BiFeO_3$, Science 326 (2009) 977–980, doi:10.1126/science.1177046.
[9] Y. Tanaka, Y. Himuro, R. Kainuma, Y. Sutou, T. Omori, K. Ishida, Ferrous polycrystalline shape-memory alloy showing huge superelasticity, Science 327 (2010) 1488–1490, doi:10.1126/science.1183169.
[10] S.H. Baek, J. Park, D.M. Kim, V.A. Aksyuk, R.R. Das, S.D. Bu, D.A. Felker, J. Lettieri, V. Vaithyanathan, S.S.N. Bharadwaja, N. Bassiri-Gharb, Y.B. Chen, H.P. Sun, C.M. Folkman, H.W. Jang, D.J. Kreft, S.K. Streiffer, R. Ramesh, X.Q. Pan, S. Trolier-McKinstry, D.G. Schlom, M.S. Rzchowski, R.H. Blick, C.B. Eom, Giant piezoelectricity on Si for hyperactive MEMS, Science 334 (2011) 958–961, doi:10.1126/science.1207186.
[11] T. Asada, Y. Koyama, Ferroelectric domain structures around the morphotropic phase boundary of the piezoelectric material $PbZr_{1-x}Ti_xO_3$, Phys. Rev. B. 75 (2007) 214111, doi:10.1103/PhysRevB.75.214111.
[12] T.A.T. Lummen, Y.J. Gu, J.J. Wang, S.M. Lei, F. Xue, A. Kumar, T.A. Barnes, E. Barnes, S. Denev, A. Belianinov, M. Holt, N.A. Morozovska, V.S. Kalinin, L.Q. Chen, V. Gopalan, Thermotropic phase boundaries in classic ferroelectrics, Nat. Comm. 5 (2014) 3172, doi:10.1038/ncomms4172.
[13] Y. Ivry, D.P. Chu, C. Durkan, Bundles of polytwins as meta-elastic domains in the thin polycrystalline simple multi-ferroic system PZT, Nanotechnology 21 (2010) 065702, doi:10.1088/0957-4484/21/6/065702.
[14] L.W. Chang, V. Nagarajan, J.F. Scott, J.M. Gregg, Self-similar nested flux closure structures in a tetragonal ferroelectric, Nano Lett 13 (2013) 2553–2557, doi:10.1021/nl400629m.
[15] A.L. Roytburd, S.P. Alpay, L.A. Bendersky, V. Nagarajan, R. Ramesh, Three-domain architecture of stress-free epitaxial ferroelectric films, J. Appl. Phys. 89 (2001) 553–556, doi:10.1063/1.1328781.
[16] Y.C.D. Ivry, J.F. Scott, E.K.H. Salje, C. Durkan, Unexpected controllable pair-structure in ferroelectric nanodomains, Nano Lett 11 (2011) 4619–4625, doi:10.1021/nl202097y.
[17] J. Paul, T. Nishimatsu, Y. Kawazoe, U.V. Waghmare, Polarization rotation, switching, and electric-field–temperature phase diagrams of ferroelectric $BaTiO_3$: a molecular dynamics study, Phys. Rev. B. 80 (2009) 024107, doi:10.1103/PhysRevB.80.024107.
[18] Y.M. Jin, Y.U. Wang, A.G. Khachaturyan, J.F. Li, D. Viehland, Adaptive ferroelectric states in systems with low domain wall energy: tetragonal microdomains, J. Appl. Phys. 94 (2003) 3629–3640, doi:10.1063/1.1599632.
[19] G.A. Schneider, T. Scholz, J. Munoz-Saldana, M.V. Swain, Domain rearrangement during nanoindentation in single-crystalline barium titanate measured by atomic force microscopy and piezoresponse force microscopy, Appl. Phys. Lett. 86 (2005) 192903, doi:10.1063/1.1920410.
[20] J.C. Agar, A.R. Damodaran, M.B. Okatan, J. Kacher, C. Gammer, R.K. Vasudevan, S. Pandya, L.R. Dedon, R.V.K. Mangalam, G.A. Velarde, S. Jesse, N. Balke, A.M. Minor, S.V. Kalinin, L.W. Martin, Highly mobile ferroelastic domain walls in compositionally graded ferroelectric thin films, Nat. Mater. 15 (2016) 549–556, doi:10.1038/nmat4567.
[21] M. Guennou, P. Bouvier, G.S. Chen, B. Dkhil, R. Haumont, G. Garbarino, J. Kreisel, Multiple high-pressure phase transitions in $BiFeO_3$, Phys. Rev. B. 84 (2011) 174107, doi:10.1103/PhysRevB.84.174107.
[22] R. Ahluwalia, N. Ng, A. Schilling, R.G.P. McQuaid, D.M. Evans, J.M. Gregg, D.J. Srolovitz, J.F. Scott, Manipulating ferroelectric domains in nanostructures under electron beams, Phys. Rev. Lett. 111 (2013) 165702, doi:10.1103/PhysRevLett.111.165702.
[23] S. Daniel, V. Daniel, M. Gil, The size-dependent ferroelectric phase transition in $BaTiO_3$ nanocrystals probed by surface plasmons, ACSnano 5 (2011) 507–515, doi:10.1021/nn102385e.
[24] C.R. Robinson, K.W. White, P. Sharma, Elucidating the mechanism for indentation size-effect in dielectrics, Appl. Phys. Lett. 101 (2012) 122901, doi:10.1063/1.4753799.
[25] V.B. Ozdol, C. Gammer, X.G. Jin, P. Ercius, C. Ophus, J. Ciston, A.M. Minor, Strain mapping at nanometer resolution using advanced nano-beam electron diffraction, Appl. Phys. Lett. 106 (2015) 253107, doi:10.1063/1.4922994.
[26] H.G. Liao, D. Zherebetskyy, H.L. Xin, C. Czarnik, P. Ercius, H. Elmlund, M. Pan, L.W. Wang, H.M. Zheng, Facet development during platinum nanocube growth, Science 345 (2014) 916–919, doi:10.1126/science.1253149.
[27] M. Ahart, M. Somayazulu, R.E. Cohen, P. Ganesh, P. Dera, H.K. Mao, R.J. Hemley, Y. Ren, P. Liermann, Z.G. Wu, Origin of morphotropic phase boundaries in ferroelectrics, Nature 451 (2008) 545–548, doi:10.1038/nature06459.
[28] A.L. Roytburd, Thermodynamics of polydomain heterostructures. I. Effect of macrostresses, J. Appl. Phys. 83 (1998) 228–238, doi:10.1063/1.366677.
[29] A.L. Roytburd, Thermodynamics of polydomain heterostructures. II. Effect of microstresses, J. Appl. Phys. 83 (1998) 239–245, doi:10.1063/1.366678.
[30] J. Zhu, X.H. Wei, Y. Zhang, Y.R. Li, Study on interfacial strain behavior of functional oxide heterostructures, J. Appl. Phys. 100 (2006) 104106, doi:10.1063/1.2375014.
[31] G. Stan, S. Krylyuk, A.V. Davydov, I. Levin, R.F. Cook, Ultimate bending strength of Si nanowires, Nano Lett. 12 (2012) 2599–2604, doi:10.1021/nl300957a.
[32] D.C. Lupascu, Y.A. Genenko, N. Balke, Aging in ferroelectrics, J. Am. Ceram. Soc. 89 (2006) 224–229, doi:10.1111/j.1551-2916.2005.00663.x.
[33] A.M. David, N. Naoyuki, O. Akira, L.G. John, Y.H. Harold, Atomic-scale imaging of nanoengineered oxygen vacancy profiles in $SrTiO_3$, Nature 430 (2004) 657–661, doi:10.1038/nature02756.

[34] W.T. Lee, E.K.H. Salje, A chemical turnstile, Appl. Phys. Lett. 87 (2005) 143110, doi:10.1063/1.2084339.
[35] C.L. Jia, K. Urban, Atomic-Resolution measurement of oxygen concentration in oxide materials, Science 303 (2004) 2001–2004, doi:10.1126/science.1093617.
[36] N.T. Tsou, P.R. Potnis, J.E. Huber, Classification of laminate domain patterns in ferroelectrics, Phys. Rev. B. 83 (2011) 184120, doi:10.1103/PhysRevB.83.184120.
[37] N. Balke, S. Jesse, A.N. Morozovska, E. Eliseev, D.W. Chung, Y. Kim, L. Adamczyk, R.E. Garc, N. Dudney, S.V. Kalinin, Nanoscale mapping of ion diffusion in a lithium-ion battery cathode, Nat. Nanotechnol. 5 (2010) 749–754, doi:10.1038/nnano.2010.174.
[38] Q. Qiao, Y. Zhang, R. Contreras-Guerrero, R. Droopad, S.T. Pantelides, S.J. Pennycook, S. Ogut, R.F. Klie, Direct observation of oxygen-vacancy-enhanced polarization in a $SrTiO_3$-buffered ferroelectric $BaTiO_3$ film on GaAs, Appl. Phys. Lett. 107 (2015) 201604, doi:10.1063/1.4936159.
[39] S. Serrano, C. Duque, P. Medina, A. Stashans, Oxygen-vacancy defects in $PbTiO_3$ and $BaTiO_3$ crystals: a quantum chemical study, Adv. Org. Inorg. Opt. Mater. 5122 (2003) 287–294, doi:10.1117/12.515777.
[40] M.J. Polking, M.G. Han, A. Yourdkhani, V. Petkov, C.F. Kisielowski, V.V. Volkov, Y. Zhu, G. Caruntu, A.P. Alivisatos, R. Ramesh, Ferroelectric order in individual nanometrescale crystals, Nat. Mater. 10 (2012) 1038, doi:10.1038/nmat3371.
[41] A. Schilling, T.B. Adams, R.M. Bowman, J.M. Gregg, G. Catalan, J.F. Scott, Scaling of domain periodicity with thickness measured in $BaTiO_3$ single crystal lamellae and comparison with other ferroics, Phys. Rev. B. 74 (2006) 024115, doi:10.1103/PhysRevB.74.024115.
[42] G.A. Samama, Pressure and temperature dependences of the dielectric properties of the perovskites $BaTiO_3$ and $SrTiO_3$, Phys. Rev. 151 (1966) 378–386, doi:10.1103/PhysRev.151.378.
[43] L. Kong, G. Liu, W. Yang, W. Cao, An insight into the origin of low-symmetry bridging phase and enhanced functionality in systems containing competing phases, Appl. Phys. Lett. 107 (2015) 042901, doi:10.1063/1.4927550.
[44] J.J. Wang, F.Y. Meng, X.Q. Ma, M.X. Xu, L.Q. Chen, Lattice, elastic, polarization, and electrostrictive properties of $BaTiO_3$ from first-principles, J. Appl. Phys. 108 (2010) 034107, doi:10.1063/1.3462441.
[45] W. Han, J.L. Zhu, S.J. Zhang, H. Zhang, X.H. Wang, Q.L. Wang, C.X. Gao, C.Q. Jin, Phase transitions in nanoparticles of $BaTiO_3$ as functions of temperature and pressure, J. Appl. Phys. 113 (2013) 193513, doi:10.1063/1.4806996.
[46] A.K. Kalyani, D.K. Khatua, B. Loukya, R. Datta, A.N. Fitch, A. Senyshyn, R. Ranjan, Metastable monoclinic and orthorhombic phases and electric field induced irreversible phase transformation at room temperature in the lead-free classical ferroelectric $BaTiO_3$, Phys. Rev. B. 91 (2015) 104104, doi:10.1103/PhysRevB.91.104104.
[47] J.L. Zhu, W. Han, H. Zhang, Z. Yuan, X.H. Wang, L.T. Li, C.Q. Jin, Phase coexistence evolution of nano $BaTiO_3$ as function of particle sizes and temperatures, J. Appl. Phys. 112 (2012) 064110, doi:10.1063/1.4751332.
[48] U.D. Venkateswaran, V.M. Naik, R. Naik, High-pressure raman studies of polycrystalline $BaTiO_3$, Phys. Rev. B. 58 (1998) 14256 -14160, doi:10.1103/PhysRevB.58.14256.
[49] S. Tyagi, V.G. Sathe, G. Sharma, V. Srihari, H.K. Poswal, Evidence of low-symmetry phases in pressure dependent Raman spectroscopic study of $BaTiO_3$, J. Mater. Sci. 53 (2018) 7224–7232, doi:10.1007/s10853-018-2102-1.
[50] J.F. Scott, M. Dawber, Oxygen-vacancy ordering as a fatigue mechanism in perovskite ferroelectrics, Appl. Phys. Lett. 76 (2000) 3801–3803, doi:10.1063/1.126786.
[51] S.E. Park, T. Shrout, Relaxor based ferroelectric single crystals for electromechanical actuators, Mater. Res. Innov. 1 (1997) 20, doi:10.1007/s100190050014.
[52] J. Gao, X. Ke, M. Acosta, J. Glaum, X. Ren, High piezoelectricity by multiphase coexisting point: barium titanate derivatives, MRS Bull. 43 (2018) 595–599, doi:10.1557/mrs.2018.155.
[53] M.H. Zhang, K. Wang, J.S. Zhou, J.J. Zhou, X.C. Chu, X. Lv, J.G. Wu, J.F. Li, Thermally stable piezoelectric properties of (K, Na)NbO_3-based lead-free perovskite with rhombohedral-tetragonal coexisting phase, Acta Mater. 122 (2017) 344–351, doi:10.1016/j.actamat.2016.10.011.